NANO LETTERS

pubs.acs.org/NanoLett

Localized Magnetic Fields in Arbitrary Directions Using Patterned Nanomagnets

Robert P. G. McNeil,*,† R. Jeff Schneble,† Masaya Kataoka,† Christopher J. B. Ford,† Takeshi Kasama,‡ Rafal E. Dunin-Borkowski,‡,∥ Joshua M. Feinberg,§,⊥ Richard J. Harrison,§ Crispin H. W. Barnes,† Desmond H. Y. Tse,† Theodossis Trypiniotis,† J. Anthony C. Bland,† David Anderson,† Geb A. C. Jones,† and Michael Pepper†

†Cavendish Laboratory, ‡Department of Materials Science and Metallurgy, and §Department of Earth Sciences, University of Cambridge, Cambridge, U.K., ∥Center for Electron Nanoscopy, Technical University of Denmark, DK-2800 Kongens Lyngby, Denmark, and ⊥Department of Geology and Geophysics, University of Minnesota, Minneapolis, MN

ABSTRACT Control of the local magnetic fields desirable for spintronics and quantum information technology is not well developed. Existing methods produce either moderately small local fields or one field orientation. We present designs of patterned magnetic elements that produce remanent fields of 50 mT (potentially 200 mT) confined to chosen, submicrometer regions in directions perpendicular to an external initializing field. A wide variety of magnetic-field profiles on nanometer scales can be produced with the option of applying electric fields, for example, to move a quantum dot between regions where the magnetic-field direction or strength is different. We have confirmed our modeling by measuring the fields in one design using electron holography.

KEYWORDS Magnetic field, nanomagnet, permalloy, electron holography

Surface split-gate technology,[1,2] with controllable local electric fields on nanometer length scales, has revolutionized quantum electronics, allowing the manipulation of even single electrons.[3−5] Spatially patterned magnetic films have a long history, for example, in bubble memory,[6] but on scales required for spintronic and quantum information technology, techniques are less well developed. Larger fields may be produced by magnetically hard materials or larger ferromagnets.[7−12] These all produce a local field parallel to the external field. Strip lines, the other common approach, produce only moderately small fields.[14−16] In the present work, we show how multiple arbitrary static field directions and strengths may be set up in specific regions.

Magnetic structures patterned on nanometer length scales, nanomagnets,[17,18] exhibit behavior different from that seen in larger ferromagnetic systems,[19,20] and so allow greater flexibility in designing and incorporating fields into small structures. For our purposes, the most relevant feature of such small magnets is that their lowest-energy configuration can be a single domain rather than a conventional flux-closure state in which the flux forms closed loops entirely within the magnet, minimizing the stray field outside. Additionally, if one sample dimension is large with respect to the others, shape anisotropy causes the magnetization to align preferentially in this direction.[21]

In this letter, we present designs of patterned magnetic elements that produce remanent fields confined to chosen, submicrometer regions, in directions perpendicular to an external initializing field. This technique can be tailored to produce a wide variety of magnetic-field profiles on nanometer scales with the option of applying electric fields, for example, to move a quantum dot between regions where the magnetic-field direction or strength is different as proposed and demonstrated by the experiments of Pioro-Ladrière et al.[12,13] We have fabricated one such design in permalloy and confirmed the accuracy of the modeling by measuring the fields using electron holography.

Figure 1a is a bright-field transmission electron microscopy (TEM) image of a nanomagnetic element design. Once initialized using an applied field $\mathbf{B}_0$ in the direction indicated, the magnetization state at remanence (i.e., that which remains once the applied field, $\mathbf{B}$ is reduced to zero) that the nanomagnets adopt follows the curved arrows. The magnetization in the central sections remains parallel to the initialization field, while the magnetization in the fingers, due to their reduced dimensions and resulting shape anisotropy, assumes an orientation parallel to their boundaries. The thickness and width of the fingers are limited to prevent flux-closure states. Finger spacing is similarly important; for widely spaced fingers there is proportionately less magnetic material to produce the field in the desired region, but fingers that are too closely spaced will form a "composite magnet" with flux-closure loops and little external stray field.

The elements in Figure 1a are designed to produce, in the gaps between the elements, an in-plane stray-field compo-

* To whom correspondence should be addressed. E-mail: rpgm2@cam.ac.uk.
Received for review: 09/7/2009
Published on Web: 04/08/2010

DOI: 10.1021/nl902949v | *Nano Lett.* **2010,** *10,* 1549–1553

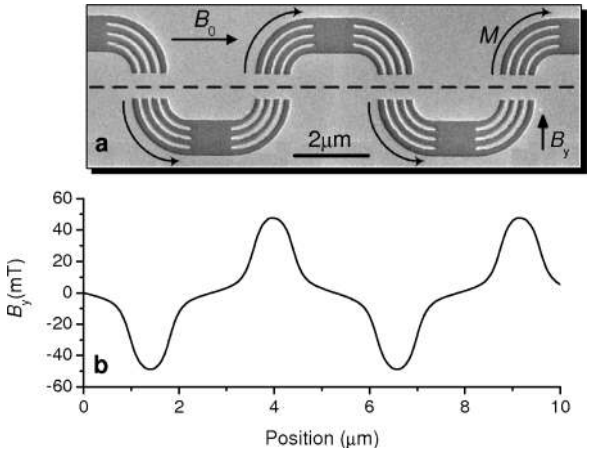

FIGURE 1. (a) Bright-field TEM image of permalloy nanomagnetic elements. An applied field, B_0, is used to initialize the structures after which the magnetization state at remanence is parallel to the curved arrows. (b) Plot of the simulated magnetic field, B_y perpendicular to B_0, as a function of position along the dashed line in (a). Because of symmetry the field perpendicular to B_y is negligible, <2 mT.

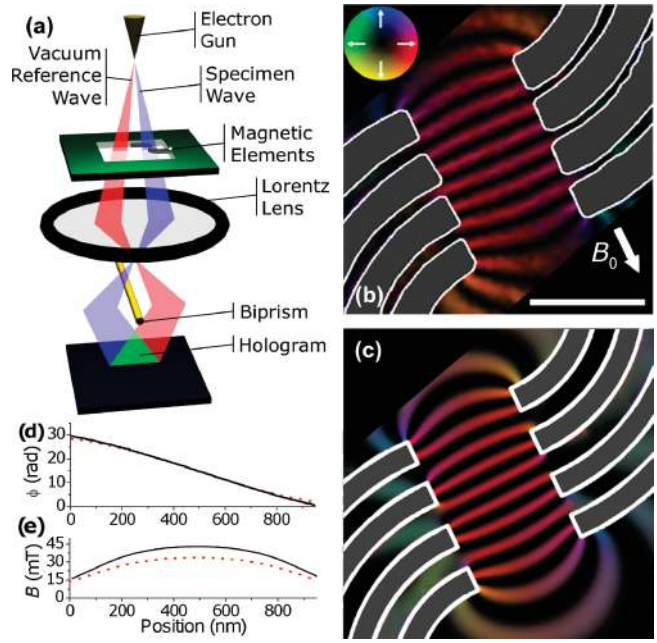

FIGURE 2. (a) Schematic diagram of electron-holography (EH) measurement. Part of electron wave passes through magnetic area of interest, the rest through a vacuum. Recombination with Lorentz lens and a biprism results in interference pattern, or hologram. Cosine-contour plot of EH phase shift in region between magnetic elements from (b) experiment and (c) computer simulation. Color scale indicates direction of magnetic flux, scale bar is 500 nm. (d) Experimental (solid line) and simulated (dotted line) EH phase shift, along the center-line of the gap shown in (b). (e) Magnetic field along center-line of sample for line running in plane of fingers (solid line) and 100 nm below (dotted line).

nent $\mathbf{B}_y$ perpendicular to $\mathbf{B}_0$. A plot of simulated $\mathbf{B}_y$ along the center line of this gap is shown in Figure 1b. This design provides the experimental flexibility for a single global field $\mathbf{B}_0$ to initialize regions of opposite field directions ($\pm y$). We will later describe designs in which a global initializing in-plane field produces an out-of-plane field at remanence (Figure 3e), while regions where a field is required parallel to $\mathbf{B}_0$ can be trivially achieved by placing magnetic elements parallel to that direction. As with existing patterned surface gates, voltages may be applied to the elements to produce electric fields defining channels and dots and to manipulate charges by moving them between regions of high- and low-magnetic field.[12] The size of the elements and local extent of the fields would allow arrays of magnetic fields to be created on useful length scales, comparable to the confinement in optical tweezers or for inclusion in micro- and nanofluidic systems. This approach may also lend itself to use in nanoelectromechanical systems, as magnetic catches or assembly aids, for example.

To validate the modeling and fabrication, the magnetic field produced by a set of permalloy elements was measured using electron holography (EH),[22,23] a transmission electron-microscopy (TEM) technique depicted schematically in Figure 2a. The difference in phase shift between a vacuum reference wave and another part of the same electron wave that has passed through the specimen is used to determine information regarding the magnetic field of the specimen through which the electrons have passed. The gradient of the measured phase shift is an integral of the in-plane component of the magnetic field along the path of the electron beam, and additional techniques are required to deduce three-dimensional magnetic-field information from this data. The TEM-imaged devices were fabricated on 50 nm thick SiN membranes from Agar Scientific. A double-layer PMMA resist was exposed with a Leica Vectorbeam UHR electron-beam lithography system. The thermally evaporated metal consisted of a 100 nm layer of permalloy ($Ni_{80}Fe_{20}$) capped with a 3 nm layer of Au. EH measurements used a Philips CM300 field-emission-gun TEM, operated at 300 kV. Holograms were acquired at remanence after saturating the sample parallel or antiparallel to the sample length with a field of ~2 T.

Figure 2b is a cosine-contour plot of the measured EH phase shift in a region between the elements shown in Figure 1a. (A cosine-contour plot is obtained by plotting $\phi' = \cos(\alpha\phi)$, where ϕ is the phase shift and α a constant "amplification" factor.) The contours indicate regions of equal phase shift, separated from each other by equal amounts of magnetic flux and are analogous to magnetic field lines. It can clearly be seen that a region of uniform magnetic field is indeed present midway between the fingers, and that this field is perpendicular to $\mathbf{B}_0$. To determine the magnitude of this field, fitting of the EH phase-shift data to a nanomagnetic simulation is required.

Previous techniques for extracting quantitative information from EH data usually either made simplifying assumptions, such as that the magnetic field is distributed uniformly throughout the sample thickness and exists nowhere else, an approximation that can be justified only for very thin

DOI: 10.1021/nl902949v | *Nano Lett.* **2010,** *10,* 1549–1553

films where the out-of-plane anisotropy forces the magnetization state to lie in the plane, or were obtained from multiple holograms at different specimen tilt angles, compiling a three-dimensional picture of the field in the region of interest.[24]

In the technique presented here, the nanomagnets are modeled using Oommf[25] or the commercially available LLG[26] package and the EH phase shift, calculated at each point in the image plane, is then compared with the measured values using the thickness of the magnetic material as the fitting parameter. Additionally Oommf was used for optimizing the device design and for the prediction of magnetic field profiles, such as the data presented in Figure 1b. While the thickness of the evaporated permalloy was 100 nm, oxidation or degradation may decrease the effective magnetic thickness of the film from the ideal case. The magnetic thickness that gives the best simulated fit to the measurements will thus be less than the actual thickness. Once a realistic model that reproduces the two-dimensional EH phase shift has been found, one can be confident that the three-dimensional field distribution predicted by the model will accurately represent that of the device being imaged. The best-fit thickness for the measured device is found to be 55 nm. Figure 2c shows a cosine-contour plot calculated for 62 nm thickness. The simulated contours closely reproduce those measured (Figure 2b). Figure 2d shows measured and simulated (for 55 nm thickness) phase shifts along the center-line of the fingers in Figure 2b. These lines are almost indistinguishable between the fingers, indicating that our models faithfully reproduce the experiment. We can now calculate the stray field produced at any point in three-dimensional space by our nanomagnetic elements.

Figure 2e plots magnetic field along the center-line of the sample in Figure 2b, both directly between, and 100 nm below, the sample. This latter plot is useful in determining the field obtainable in a two-dimensional electron gas (2DEG), for magnetic elements patterned on top of a typical GaAs/AlGaAs heterostructure, commonly used in quantum electronics. It can be seen that the reduction in field strength at this depth is moderate; this is also a necessity in schemes such as those of Appelbaum[27] where magnetic fields must be applied to layered structures and Barnes[28] where a local field extends down to passing quantum dots which form spin qubits.

Previous measurements of patterned discs and pillars in dysprosium[7,8] produced fields of up to 400 mT but involved just the out-of-plane component of the magnetic field. The effect of the Dy magnets in the work of Ye et al.[9] was the addition of a periodic magnetic field parallel to the applied field with an amplitude in the underlying 2DEG of ~10 mT. However, dysprosium is only suitable for single-field directions due to its large coercive field. Larger magnetic stripes and rectangular shapes have also been measured,[10,11] producing out-of-plane fields in the 2DEG of up to 500 mT; however, the elements used had in-plane dimensions of tens to hundreds of micrometers and produced fields over extended rather than localized regions.

Permalloy is a magnetically soft material and for a given element will produce a smaller maximum field. However, the small coercive field allows the magnetization to realign, giving the transverse fields of Figure 1b. Harder materials such as cobalt can produce larger fields[10] and so are good choices where fields parallel to an initializing field are required. However, in our simulations with cobalt, the magnetization was not fully aligned to the curved fingers when the initializing field was removed and consequently these elements gave smaller transverse fields. Some other materials may be suitable; in our simulations, iron was found to give ~1.6 times the field of permalloy but with less good confinement.

The magnetic structures presented here produce an in-plane field at remanence that is chosen to be perpendicular to the field used for initialization. The field is concentrated in an area ~0.5 μm^2, and oscillates with an in-plane peak-to-peak amplitude of ~90 mT between the magnets and ~60 mT at the depth of a typical 2DEG. Unwanted stray fields outside this region are minimal, as most of the magnetic flux is channelled from one magnetic element to the next; this type of stray-field control may be of great benefit in spintronic devices and is a capability that has not previously been explored.

Figure 3a,b show nanomagnetic elements capable of producing fields in multiple in-plane directions using a single reversible applied field. Figure 3c shows the effect of polarizing such elements and then gradually applying a reverse field. The central broad sections of elements such as those in Figure 1a are less anisotropic than the fingers and so allow for selective reversal of the magnetization of specific elements. Elements with continuous fingers that are not joined to form a "body" region, such as those in Figure 3a, require a larger coercive field to switch their magnetization; compare the elements in Figure 3c (ii and iii) at 40 mT. The solid sections of the S-shaped elements reverse easily from "E" to "W" polarization and are then stable to higher fields, whereas the finger regions resist depolarisation, allowing E and W regions to coexist; Figure 3b. Being able to switch different elements at different fields allows greater control in designing magnetic profiles. Figure 3d shows in cross-section how existing split-gate technology can be used to vary the field direction electrically. Applying different voltages to the asymmetrically placed electrostatic gates shifts the potential minimum defining a channel or quantum dot to produce a 90° rotation of the local field. Figure 3e shows a different style of element used to create a stronger out-of-plane field. It too is initialized with an in-plane field and produces fields >80 mT over an area of 0.5 μm^2 100 nm below the plane of the magnets. Inter-

DOI: 10.1021/nl902949v | Nano Lett. 2010, 10, 1549–1553

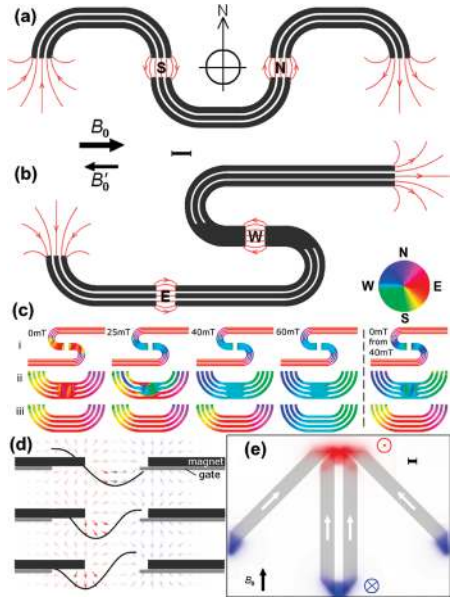

FIGURE 3. (a,b) Schematic nanomagnetic elements used to create fields in multiple directions N, S, E, and W from a single reversible field B_0. (b) Field at W is produced by an initial B_0 followed by smaller reverse field B'_0. (c) Simulated sections of (a and b) at different reverse fields B'_0. Elements initially saturated at B_0. Color represents magnetic direction as shown. The higher coercive fields of narrow slotted sections allows selective switching. By 40 mT one C-shaped element has reversed while its slotted counterpart has not. Rightmost elements show configuration at remanence after applying 40 mT. (d) Example of asymmetric electrostatic gates (gray) used to select field from magnetic elements (black) by shifting the potential minimum. (e) Magnetic element arrangement producing out-of-plane field below magnets from the same B_0 used in (a−c). Red and blue indicate field into and out of the page. Angled elements constrain the parallel ones preventing antiparallel magnetic configuration and increasing field strength. All scale bars are 500 nm.

mediate field directions can be produced by variations on these designs.

Larger fields may also be achieved by improved alignment of the magnetization in the fingers, a reduction in the gap between fingers or an increased thickness of deposited material. Our simulations predict that fields greater than 200 mT are possible with other materials, such as iron, using geometries similar to those shown here. Empirically, for simmulated elements of thickness T and gap width G, the field B is given by $(B/mT) = m \times (T/G) + c$, where m is a constant and c is an offset, with $(m, c) = (430, -11)$ for Fe and (230, 3) for permalloy. This holds for thicknesses up to ∼120 nm (above which flux-closure domains form within the elements), and for gap widths above ∼300 nm (Fe) and ∼120 nm (permalloy). This indicates that the flux spreads vertically over a region roughly equal to the gap width G.

In conclusion, the nanomagnets presented here can produce controlled local magnetic fields in multiple arbitrary directions in the absence of an applied field, through the use of a single global initialization field. The stray field produced can be confined to desired submicrometer regions and electrostatic gates used to move electrons between regions of different magnetic direction and field strength. The ease with which this design can be tailored to produce arbitrary field profiles and the possibility of electrostatic and magnetic gate integration mean this work may be useful in a wide range of spintronic and nanoelectromechanical applications, or anywhere localized fields or field gradients[12] are required.

Acknowledgment. This research is part of QIP IRC www.qipirc.org and is funded by the U.K. EPSRC. The authors also thank CamGrid for computing resources. In memoriam, J. A. C. Bland.

REFERENCES AND NOTES

(1) Thornton, T. J.; Pepper, M.; Ahmed, H.; Andrews, D.; Davies, G. J. One dimensional conduction and inelastic scattering in GaAs-AlGaAs heterojunctions. *Phys. Rev. Lett.* **1986**, *56*, 1198–1201.
(2) Ford, C. J. B.; Thornton, T. J.; Newbury, R.; Pepper, M.; Ahmed, H.; Peacock, D. C.; Ritchie, D. A.; Frost, J. E. F.; Jones, G. A. C. Electrostatically defined heterojunction rings and the Aharonov-Bohm effect. *Appl. Phys. Lett.* **1989**, *54*, 21–23.
(3) Field, M.; et al. Measurement of Coulomb blockade with a non-invasive voltage probe. *Phys. Rev. Lett.* **1993**, *70*, 1311–1314.
(4) Elzerman, J. M.; et al. Single-shot read-out of an individual electron spin in a quantum dot. *Nature* **2004**, *430*, 431–435.
(5) Kouwenhoven, L. P.; Austing, D. G.; Tarucha, S. Few-electron quantum dots. *Rep. Prog. Phys.* **2001**, *64*, 701–736.
(6) Bobeck, A. H. Magnetic Bubble Devices. *J. Vac. Sci. Technol.* **1972**, *9*, 1145.
(7) Ye, P. D.; Weiss, D.; von Klitzing, K.; Eberl, K.; Nickel, H. Fabrication and characterization of micromagnetic arrays on top of GaAs/AlGaAs heterostructures. *Appl. Phys. Lett.* **1995**, *67*, 1441–1443.
(8) Novoselov, K. S.; Geim, A. K.; Dubonos, S. V.; Cornelissens, Y. G.; Peeters, F. M.; Maan, J. C. Quenching of the Hall effect in localised high magnetic field regions. *Physica E* **2002**, *12*, 244–247.
(9) Ye, P. D.; et al. Electrons in a periodic magnetic field induced by a regular array of micromagnets. *Phys. Rev. Lett.* **1995**, *74*, 3013–3016.
(10) Kubrak, V.; Neumann, A.; Gallagher, B. L.; Main, P. C.; Henini, M. Magnetoresistance and Hall magnetometry of single submicron ferromagnetic structures. *J. Appl. Phys.* **2000**, *87*, 6986–5988.
(11) Monzon, F. G.; Johnson, M; Roukes, M. L. Strong Hall voltage modulation in hybrid ferromagnet/semiconductor microstructures. *Appl. Phys. Lett.* **1997**, *71*, 3087–3089.
(12) Pioro-Ladrière, M.; et al. Electrically driven single-electron spin resonance in a slanting Zeeman field. *Nat. Phys.* **2008**, *4*, 776.
(13) Pioro-Ladrière, M.; Tokura, Y.; Obata, T.; Kubo, T.; Tarucha, S. Micromagnets for coherent control of spin-charge qubit in lateral quantum dots. *Appl. Phys. Lett.* **2007**, *90*, No. 024105.
(14) Machida, T.; Yamazaki, T.; Ikushima, K.; Komiyama, S. Coherent control of nuclear-spin system in a quantum-Hall device. *Appl. Phys. Lett.* **2003**, *82*, 409–411.
(15) Yusa, G.; Muraki, K.; Takashina, K.; Hashimoto, K.; Hirayama, Y. Controlled multiple quantum coherences of nuclear spins in a nanometre-scale device. *Nature* **2005**, *434*, 1001–1005.
(16) Koppens, F. H. L.; et al. Driven coherent oscillations of a single electron spin in a quantum dot. *Nature* **2006**, *442*, 766–771.
(17) Cowburn, R. P.; Koltsov, D. K.; Adeyeye, A. O.; Welland, M. E. Single-Domain circular Nanomagnets. *Phys. Rev. Lett.* **1999**, *83*, 1042–1045.
(18) Chien, C. L.; Zhu, F. Q.; Zhu, J. G. Patterned nanomagnets. *Phys. Today* **2007**, *60*, 40–45.
(19) Stoner, E. C.; Wohlfarth, E. P. A mechanism of magnetic hysteresis in heterogeneous alloys. *Philos. Trans. R. Soc. London, Ser. A* **1948**, *240*, 599–642.
(20) Frei, E. H.; Brown, W. F. Micromagnetic and Fine Particles. *J. Appl. Phys.* **1968**, *39*, 993–994.

DOI: 10.1021/nl902949v | *Nano Lett.* **2010,** *10,* 1549–1553

(21) *Ultrathin Magnetic Structures I*; Bland, J. A. C., Heinrich, B., Eds.; Springer-Verlag: New York, 1994; Chapter 1.
(22) Dunin-Borkowski, R. E.; et al. Off-axis electron holography of magnetic nanowires and chains, rings and planar arrays of magnetic nanoparticles. *Microsc. Res. Tech.* **2004**, *64*, 390–402.
(23) Tonomura, A. Electron-holographic interference microscopy. *Adv. Phys.* **1992**, *41*, 59–103.
(24) Lai, G.; et al. Three-dimensional reconstruction of magnetic vector fields using electron-holographic interferometry. *J. Appl. Phys.* **1994**, *75*, 4593–4598.
(25) Donahue, M. J.; Porter, D. G. OOMMF user's guide; Interagency Report NISTIR 6376. Tech. Rep.; National Institute of Standards and Technology: Washington, DC, 1999; http://math.nist.gov/oommf. Accessed 2007.
(26) Scheinfein, M. R. *LLG Micromagnetics Simulator* http://llgmicro.home.mindspring.com. Accessed 2007.
(27) Appelbaum, I.; Huang, B.; Monsma, D. J. Electronic measurement and control of spin transport in silicon. *Nature* **2007**, *447*, 295–298.
(28) Barnes, C. H. W.; Shilton, J. M.; Robinson, A. M. Quantum computation using electrons trapped by surface acoustic waves. *Phys. Rev. B.* **2000**, *62*, 8410–8419.

DOI: 10.1021/nl902949v | *Nano Lett.* **2010,** *10,* 1549--1553